Materials Chemistry and Physics 134 (2012) 631–638

Contents lists available at SciVerse ScienceDirect

Materials Chemistry and Physics

journal homepage: www.elsevier.com/locate/matchemphys

In situ-Raman studies on thermally induced structural changes of porous MoO_3 prepared in vapor phase under He and H_2

D.E. Diaz-Droguett [a,*], R. El Far [a], V.M. Fuenzalida [b], A.L. Cabrera [a]

[a] Departamento de Física, Facultad de Física, Pontificia Universidad Católica de Chile, Santiago, Chile
[b] Departamento de Física, Facultad de Ciencias Físicas y Matemáticas, Universidad de Chile, Santiago, Chile

ARTICLE INFO

Article history:
Received 7 December 2011
Received in revised form
12 March 2012
Accepted 15 March 2012

Keywords:
Porous MoO_3
Raman
Structure
Helium
Hydrogen
Laser irradiation

ABSTRACT

The structural transformations induced by heating on MoO_3 mesoporous samples grown in vapor-phase under helium and hydrogen were studied by in situ Raman spectroscopy. The samples were continuously irradiated by a He–Ne laser of 5.5 mW for 105 min and Raman spectra were dynamically acquired every 5 min, in order to evaluate the laser effects. The He-grown sample did not undergo structural transformations due to the laser irradiation while the H_2-grown sample underwent changes after just 10 min of irradiation. On the other hand, each type of sample was heated in air from room temperature up to 450 °C using a heating rate of 5 °C min^{-1} and Raman spectra were recorded each 25 °C. The He-grown sample remained structural unchanged up to 250 °C revealing a high temperature state of its amorphous matrix whereas the H_2-grown sample exhibited changes around 70 °C. These changes were attributed to the crystallization onset of its amorphous matrix to β-MoO_3. However, this same transition was detected between 250 °C and 275 °C for the He-grown sample. A second transformation was detected in both samples in a temperature range more similar associated to the transition of the formed β-MoO_3 phase to α-MoO_3. After the heat treatment, the oxide of both samples was slightly reduced, as revealed by XPS analysis.

The metastability at low temperatures of the amorphous phase of the H_2-grown sample could be associated to release of hydrogen trapped inside the compound and to the break of weak bonds between Mo and OH groups. At high temperatures, above 225 °C, the rapid conversion to β-MoO_3 of the amorphous matrix of the H_2-grown sample occurred due to the dehydration of the sample.

1. Introduction

Porous materials of transition metal oxides are promising materials for fields such as catalysis, gas sensing and bioreactors [1,2]. This is because their inherent pore structure confers them a high reactivity and because of the particular electronic configuration of the metal cation. Its incomplete d-shell leads to metal–oxygen bonding varying from nearly ionic to metallic [3]. Among transition metal oxides, MoO_3 has considerable importance by its catalytic activity in the selective oxidation of hydrocarbons [4–6] as well as by its application as active element in conductance-type gas sensors [7]. In fact, MoO_3 has been found to be very sensitive to gases such as: H_2, NH_3, NO, NO_2 and CO in the temperature range of 300–500 °C [8–13].

MoO_3 can exist in different crystalline structures: the orthorhombic phase, α-MoO_3 [14], which is the thermodynamically stable phase, the metastable monoclinic phase, β-MoO_3 [15,16], the metastable high-pressure phase, MoO_3-II [17]; and the hexagonal phase, h-MoO_3 [18,19]. α-MoO_3 (space group *Pbmn*) has a layered structure consisting of double layers of distorted MoO_6 octahedra held together by two different covalent forces in the *a* and *c* – axes, i.e., [100] and [001] directions but by van der Waals forces in the *b*-axis alone, i.e., [010] direction. In each octahedron of MoO_6, one Mo atom is surrounded by six oxygen atoms. The octahedra of each layer share its edges forming zig-zag rows in the [100] and are connected in the [100] direction by common corners. As consequence, one oxygen is unshared while the other two oxygen atoms share common octahedra and three other oxygens are partly shared and common to three octahedra [20,21]. In contrast, β-MoO_3 (space group $P2_1/c$) has monoclinic structure similar to ReO_3 formed by corner sharing distorted MoO_6 octahedra, where no oxygen atoms singly coordinated [16,22].

Porous MoO_3 can be directly grown by condensation of MoO_3 vapor in presence of a carrier gas at low pressure [23]. This method consists in vaporizing a MoO_3 pellet using a tungsten resistive source under an atmosphere at around 100 Pa of a carrier gas.

* Corresponding author: Tel.: +56 2 3544499.
E-mail address: dodiaz@fis.puc.cl (D.E. Diaz-Droguett).

0254-0584/$ – see front matter © 2012 Elsevier B.V. All rights reserved.
doi:10.1016/j.matchemphys.2012.03.042

Under these conditions, the gas density is not enough to cool and confine the MoO_3 vapor causing a low super saturation of the vapor in the vicinity of the MoO_3 pellet or, simply avoiding reaching super saturation conditions. The poor confinement of the vapor leads to a high diffusion rate of the material away from the evaporation source and to a low coalescence rate. The small amounts of clusters formed are rapidly immobilized on a collecting surface cooled at liquid nitrogen temperature leading to the formation of porous material of amorphous matrix [24]. Diaz-Droguett et al. reported the preparation conditions which favor the growth of porous MoO_3 using helium or hydrogen as carrier gas [24].

For potential catalytic, optical recording or gas sensing applications, the temperature effect on the structural characteristics of porous MoO_3 needs to be studied. Some works on structural changes induced by heat treatments (HTs) or laser irradiation of non-porous molybdenum oxide have been reported. R. Murugan et al. reported on the structural changes of hydrated MoO_3 when it was heated in air from room temperature (RT) to 500 °C [25]. These studies were performed using mainly in situ Raman spectroscopy. M.A. Camacho-López et al. studied the amorphous–crystalline transition in hydrated MoO_3 using Raman spectroscopy by heating the samples in air in the same temperature range (25–500 °C) [26]. E. Haro-Poniatowski et al. also reported on the structural transformations of hydrated MoO_3 but induced by laser irradiation using a U1000 Jobin–Yvon double monochromator [27]. The knowledge on thermally induced structure transition routes and phase stability of MoO_3 compounds is very important in catalysis where the catalytic properties can be controlled by varying the structural characteristics of the molybdenum oxide [28]. On the other hand, if the energy threshold for inducing structural transformations in a MoO_3 compound is low, this material could be used as a high density optical storage medium [27].

In the present work, MoO_3 porous samples grown in vapor-phase under helium and hydrogen were irradiated by laser as well as heated in air from RT up to 450 °C. In both cases, the heating effects on the samples structure were dynamically studied by in situ Raman spectroscopy. The temperature ranges of the different phase transitions were determined for the different kind of samples as well as the evolution of each phase as function of temperature.

2. Experimental

2.1. Preparation of porous MoO_3

Mesoporous MoO_3 was grown in a simple one-step process by resistive evaporation of a 0.5 g MoO_3 pellet from a tungsten boat in the presence of a carrier gas: He (AGA, 99.995%, $O_2 < 5$ ppm and $H_2O < 2$ ppm) or H_2 (AGA, 99.995%, $O_2 < 5$ ppm and $H_2O < 4$ ppm). The first step of the procedure was evacuating a high vacuum chamber using a turbomolecular pump backed by a rotatory pump until a pressure of 10^{-4} Pa. This is much lower than the operation pressure and provides a clean environment; particularly avoiding oxygen in the system. A mass spectrometer was used to monitor the partial pressure of the active gases, mainly O_2, N_2, H_2O and Ar; the latter is inert, but it can affect the material growth in vapor-phase because of its mass. After evacuating the chamber, the carrier gas was injected to reach the operation pressure of 100 Pa. This pressure was maintained only whit the rotatory pump, in order to avoid excess gas flow. The operation pressure was measured with absolute (capacitive) pressure gauges.

The pellet was prepared by cold-pressing MoO_3 commercial powder (Alfa Aesar, 99.95% of purity) which it was placed on a tungsten boat of 95 mm in length, 10 mm wide and 0.1 mm thick. The boat was resistively heated using a variable transformer. The current intensity was increased until the working temperature was achieved. The boat temperature was measured with an optical pyrometer through a sapphire window. The material was collected on the cold surface of a liquid nitrogen-filled copper semi cylinder 152 mm external diameter, 3 mm thick and 300 mm long located 75 mm above the tungsten boat; this distance remains fixed for all evaporations. After the evaporation, the high vacuum chamber was left overnight to reach room temperature and ventilated with air and opened to remove the porous MoO_3 from the collector surface.

For a comparative study, three types of samples were thermally treated in air under the same conditions and analyzed by in situ Raman spectroscopy; the first sample corresponded to the commercial MoO_3 powder (source material) considered as a reference sample, the second sample was porous MoO_3 grown in helium using an evaporating boat temperature of 668 °C and the third a MoO_3 porous sample grown in hydrogen at 1196 °C, both samples prepared under the same carrier gas pressure of 100 Pa [24].

2.2. Characterization

For the Raman characterization as function of temperature, the samples in powder form were prepared as following: the powder was dispersed in isopropyl alcohol using an ultrasonic bath for 7 min. The suspension was deposited using a dropper on a glass substrate of 18 mm × 18 mm and 0.5 mm in thickness. The deposited sample was dried in air at RT forming a layer of porous material on the substrate. The set (substrate + sample) was located on a heating and cooling stage (Linkam) which can operate with temperatures between −190 and 600 °C.

Thermally induced structural changes of the samples were studied using a Raman spectrometer coupled to a microscope LabRam 010 from ISA using a He–Ne laser ($\lambda = 632.8$ nm) at 5.5 mW and without filter. The Raman system uses a backscattering geometry, where the incident beam is linearly polarized and the spectral detection unpolarized. The objective lens of the microscope was an Olympus Mplan 10× (Numerical aperture 0.9). The laser spot was about 100 μm in diameter. The HTs were carried out heating the samples in air from RT up to 450 °C with a heating rate of 5 °C min^{-1}. In situ Raman spectra were recorded each 25 °C using exposure times between 2 and 20 s. The sample remained for 5 min at each temperature but the spectrum was acquired just after 3 min.

Before the HTs, each type of sample at RT was irradiated continuously with the laser by 105 min to evaluate possible heating effects induced by the beam. In this case, the spectra were recorded dynamically every 5 min of irradiation using exposure times 20 s.

On the other hand, oxidation state information of the samples before and after the HT was obtained from X-ray photoelectron spectroscopy (XPS, Physical Electronics system model 1257), using Al K-α emission, with working pressures in the range of 10^{-6}–10^{-7} Pa, using high resolution scans (pass energy 71.55 eV and step size 0.2 eV). All spectra were analyzed using the Multipak and XPSpeak41 softwares. The energy scale was calibrated by assigning 284.8 eV to the C 1 s peak corresponding to adventitious carbon. After calibration, the background from each spectrum was subtracted using a Shirley-type background.

3. Results

The chemical, morphological and structural characteristics as well as the pore sizes of these MoO_3 mesoporous samples grown at 100 Pa in helium or hydrogen were already given in detail in ref. [24]. These samples were constituted by an amorphous matrix with nanocrystalline inclusions. Moreover, thermogravimetric studies showed that the H_2-grown porous samples were slightly hydrated corresponding to a compound of the form $MoO_3 \cdot 1/7H_2O$ whereas lattice H_2O was not detected in the He-grown porous samples [24].

3.1. MoO_3 powder

A reference spectrum from commercial α-MoO_3 powder was recorded. The assignment of the main vibrational modes, according to reference [27], is shown in Fig. 1. This spectrum recorded with the sample at RT shows the vibration region of MoO_3, between 150 and 1100 cm^{-1}. The Mo-O stretching (ν) and bending (δ) vibrations usually appear in the 1000–600 cm^{-1} and 600–150 cm^{-1} range, respectively. The wave number range, between 150 and 400 cm^{-1}, is associated to the Mo–O modes type scissor, wagging, twist and rotational/translational rigid MoO_4 chain mode [29]. In the high-wave number range, between 1000 and 600 cm^{-1}, the Raman spectrum of Fig. 1 displays three well-defined peaks located at 994, 819 and 665 cm^{-1}, attributed to the stretching vibrations: ν(O–Mo), ν(O–Mo_2) and ν(O–Mo_3), respectively. These peaks are considered the fingerprints of the α-MoO_3 phase. A complete detail of Raman lines positions for α-MoO_3 and their modes assignments can also be found in references [30,31]. Finally, the Raman peak at 994 cm^{-1} is the typical vibration of the terminal double bonds (Mo=O) and it appears as narrow band in the spectrum due to its non-polar character [26].

3.2. Laser irradiation effects on porous MoO_3

No structural changes were detected in the sample grown in He while the one grown in H_2 revealed changes under laser irradiation, as shown by the Raman spectra sequences of Fig. 2(A) and (B), respectively. The spectra a) were recorded at the beginning of the laser irradiation and the spectra b), c) and d) were acquired after 10, 45 and 105 minutes of irradiation, respectively. In both samples, all relatively sharp peaks are due to the crystalline inclusions embedded in the amorphous matrix. In Fig. 2(A), all spectra are similar exhibiting the characteristic peaks associated to the stretching modes of α-MoO_3 located at 993, 820 and 663 cm^{-1}. Moreover, two weak peaks at 850 and 776 cm^{-1} are identified in all spectra which correspond to vibrational modes of the monoclinic phase of MoO_3, named β-MoO_3 [32], indicating that a very small proportion of crystals with β-MoO_3 structure are present in the amorphous matrix of the He-grown sample, too. On the contrary, Fig. 2(B) reveals an evolution of the Raman profile induced by laser irradiation. The spectrum (a) recorded at the onset of the laser irradiation reveals a Raman profile only corresponding to α-MoO_3

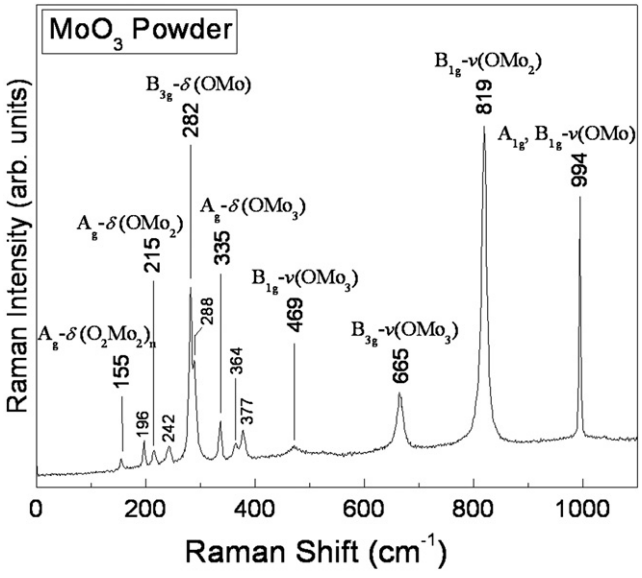

Fig. 1. Raman spectrum of MoO_3 commercial powder at RT.

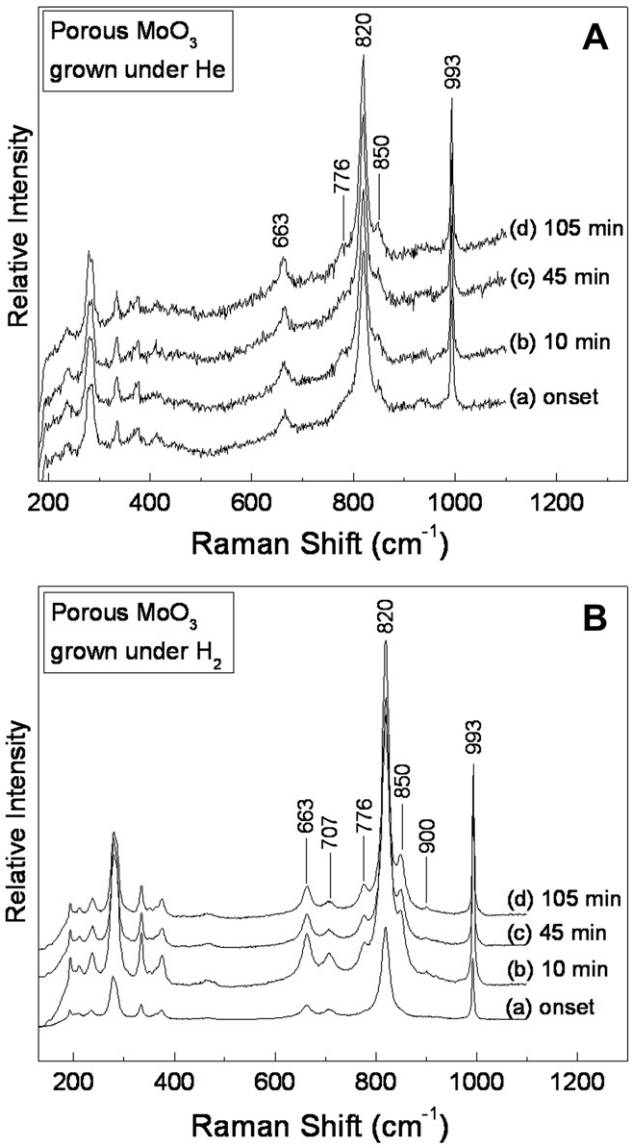

Fig. 2. Raman spectra recorded at different laser irradiation times of the porous samples grown under: (A) He and (B) H_2.

except by the peak centered at 707 cm^{-1} which could not be assigned to a defined vibration mode of MoO_3. The appearance of two small peaks centered at 850 and 776 cm^{-1} and another very weak peak located at 900 cm^{-1}, also corresponding to a vibrational mode of β-MoO_3, were caused by the irradiation effect, as revealed by the Raman spectra (b), (c), and (d) of Fig. 2B.

For evaluating the structural changes, in special, the formation of β-MoO_3 phase in the H_2-grown sample by heating effect induced by the laser, Lorentzian curve fits in the high-wave number range were carried out on all the Raman spectra. The same fits were performed on the spectra obtained during the HTs carried out with the samples. Fig. 3(a) shows a typical curve fit, in this case carried out on the spectrum recorded at 95 min of irradiation. The evolution of the area below the curve of the peaks located at 850 (orthorhombic) and 820 (monoclinic) cm^{-1} at the different irradiation times was determined through the fits, in order to study the evolution of the amount of phase formed, as shown in Fig. 3(b). The peaks around 850 and 820 cm^{-1} are the more intense Raman signals in samples composed only by a α-MoO_3 or β-MoO_3 phase,

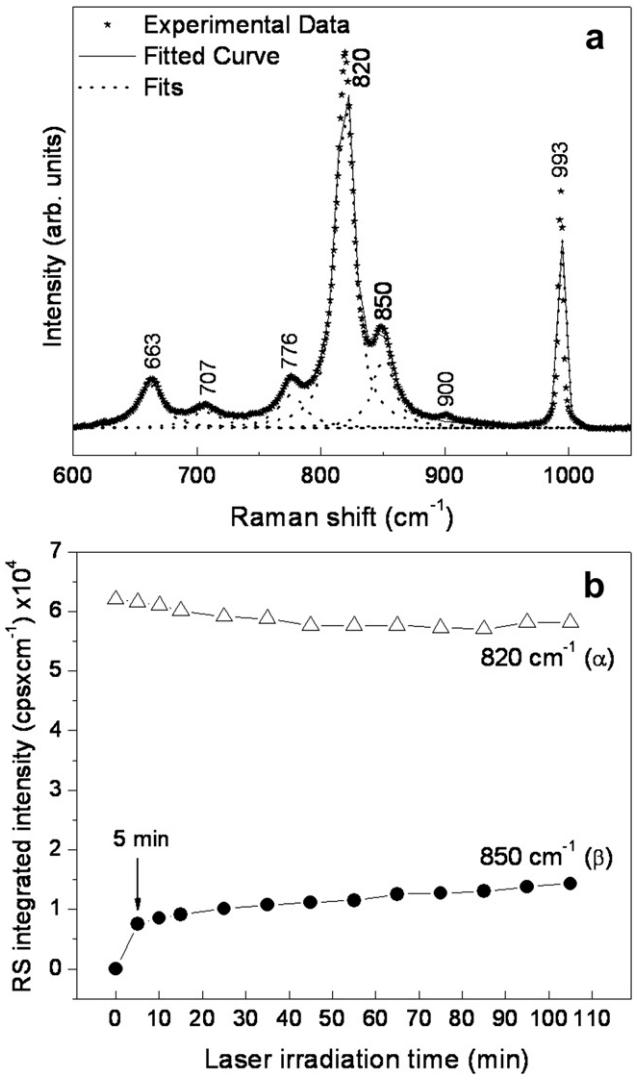

Fig. 3. (a) Typical curve fit carried out on the Raman spectra. (b) Evolution of the area below the curve of the peaks located at 850 and 820 cm^{-1} by irradiation effect.

respectively [32], for this reason these signals were chosen for the area analyses. At 5 min of irradiation, formation of β-MoO_3 phase is already detected, afterwards the amount of this phase slightly increased with the irradiation time, as revealed by the rise of the area below the curve of the peak (peak area) at 850 cm^{-1}. Formation of β-MoO_3 phase by irradiation effect would be associated to the structural transformation of the MoO_3 amorphous matrix of this porous sample. The evolution of the peak area at 820 cm^{-1} is kept practically constant.

Due to the laser induced structural changes caused by just 5 min of continuous irradiation, the sample under HT was illuminated by the beam only when the Raman spectrum needs to be acquired at a certain temperature, avoiding exposure to higher irradiation doses. In general, the acquisition times of the spectra showed in this report did not exceed 2 min.

3.3. Heat treatment effects on porous MoO_3

3.3.1. He-grown sample

Fig. 4 shows Raman spectra of the He-grown porous sample recorded during the HT from RT up to 450 °C. No structural

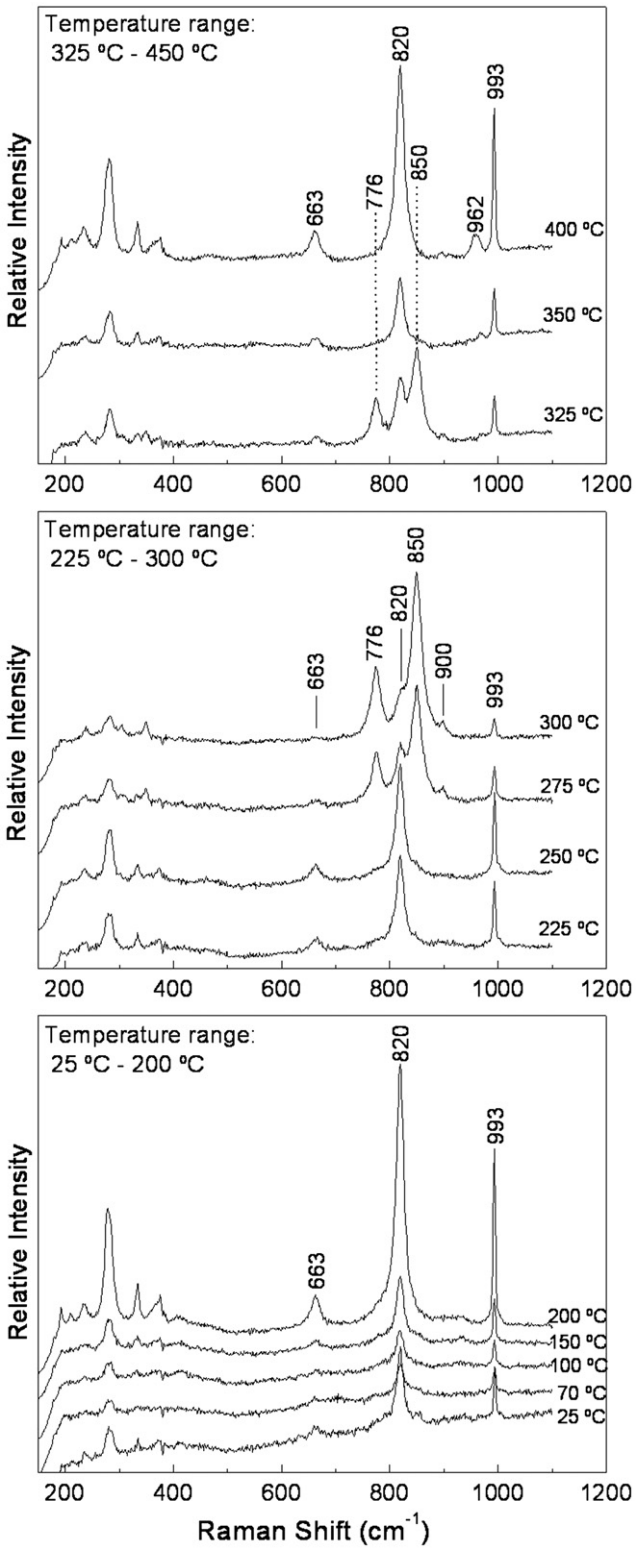

Fig. 4. Raman spectra of the He-grown porous sample obtained during the HT.

transformations were detected up to 250 °C, as revealed by spectra showing a Raman profile corresponding mainly to α-MoO_3 with their peaks characteristic of stretching modes centered at 993, 820 and 663 cm^{-1}. Between 275 and 325 °C, Raman profiles associated to the presence of intermixed α-/β-MoO_3 phases are identified, all of them showing the typical peaks of the monoclinic phase (β) at

900 (very weak), 850 and 776 cm^{-1} mixed with the peaks associated to the orthorhombic phase (α) of MoO_3. Relative intensity variations among these peaks associated to each phase are only detected in this temperature range. After 350 °C, a Raman profile corresponding only to α-MoO_3 is again identified except by a weak peak centered at 962 cm^{-1} which can not be assigned to a defined vibration mode for some phase of MoO_3. However, G. Mestl et al. [33] reported three additional Raman signals (724, 888 and 954 cm^{-1}) in the Mo–O stretching region for MoO_3 after 10 h evacuation to 10^{-1} Pa at 375 °C leading to a formation of a suboxide, MoO_{3-x}. The signal at 954 cm^{-1} was associated to the oxygen removal causing octahedra (MoO_6) being less distorted than in MoO_3 layered structure. We guess that our signal at 962 cm^{-1} would be also associated to oxygen deficient from the MoO_3 compound when the sample temperature exceeded 350 °C during the heat treatment. Finally, the spectrum acquired at 450 °C was not plotted in Fig. 4 because was very similar to the spectrum recorded at 400 °C.

Since formation of β-MoO_3 phase was detected after 250 °C, the curve fits were performed only on the Raman spectra obtained after this temperature. Fig. 5 shows the evolution of the peak area of the main signal associated to the monoclinic and orthorhombic phase of MoO_3, centered at 850 and 820 cm^{-1}, respectively. The amount of monoclinic phase formed in the He-grown sample was increasing after 250 °C up to reach a maximum value at 300 °C, as revealed by the evolution in the temperature range of the peak area at 850 cm^{-1}. The formation and increase of the monoclinic phase between 250 and 300 °C is associated to the crystallization of the amorphous matrix of this porous sample leading to the formation of new crystals with β-MoO_3 structure. After 300 °C, the amount of monoclinic phase in the sample starts to decrease up to 350 °C where the signal at 850 cm^{-1} is already not detected, as revealed by the evolution of the peak area. However, between 275 and 325 °C the amount of β-MoO_3 phase formed is always major that the amount of α-MoO_3 phase. The decrease of the amount of β-MoO_3 phase between 300 and 350 °C is associated to the conversion or transformation to α-MoO_3 of this monoclinic phase. However, the increase of the peak area of the signal at 820 cm^{-1} related to orthorhombic phase grew strongly only after 375 °C, dramatically increasing the amount of α-MoO_3 phase between 400 and 450 °C, as revealed by the evolution of the peak area of this signal.

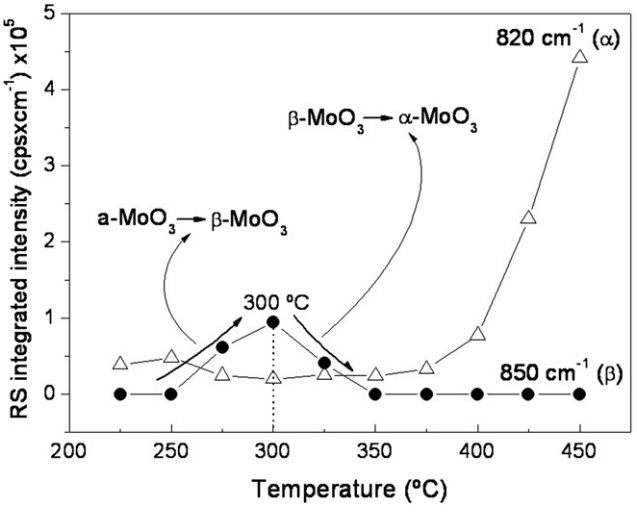

Fig. 5. Evolution of the area below the curve of the peaks located at 850 and 820 cm^{-1} by HT effect.

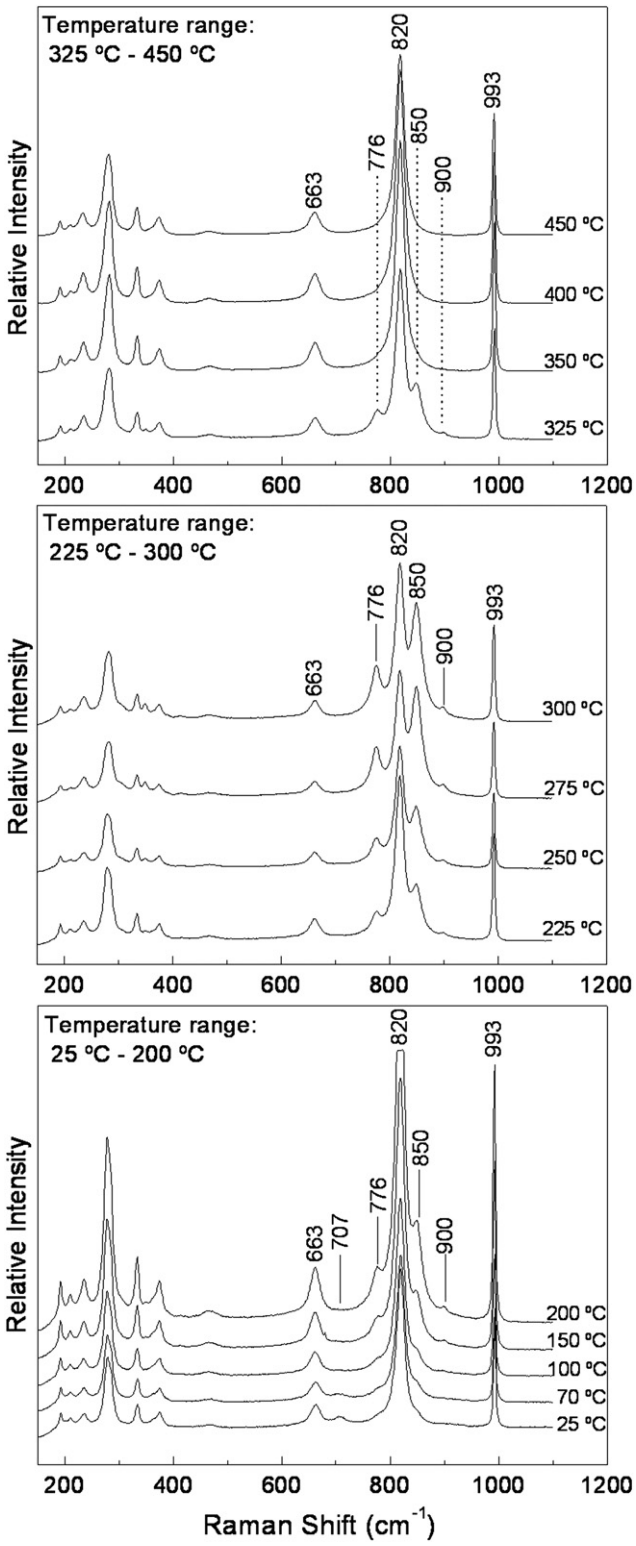

Fig. 6. Raman spectra of the H_2-grown porous sample obtained during the HT.

3.3.2. *H_2-grown sample*

Fig. 6 shows Raman spectra of the H_2-grown porous sample recorded during the HT from RT up to 450 °C. At RT, the Raman profile corresponds to α-MoO_3 except by the peak at 707 cm^{-1} which could not be identified. Opposite to the case of the He-grown sample, formation of β-MoO_3 phase is detected at temperatures as

low as 70 °C where small shoulders in the spectrum recorded at this temperature can be already detected at 850 and 776 cm^{-1}. These peaks become more defined and intense as temperature increased. Therefore, up to 325 °C, Raman profiles corresponding to mixed phases: orthorhombic and monoclinic of MoO_3 (α-/β-MoO_3) are identified. At 350 °C, peaks at 850 and 776 cm^{-1} are not detected in the spectrum indicating that the β-MoO_3 phase is not present in the sample. Therefore, from 350 and up to 450 °C, the Raman spectra only show vibrational modes associated to α-MoO_3. In the case of this H_2-grown sample, peak at 962 cm^{-1} was not detected when the temperature exceeded to 350 °C as compared with the case of the He-grown sample. By the moment we do not have explanation for this fact.

Since the structural changes occurred in the H_2-grown sample at early temperatures, the values of the peak area of the signals at 850 and 820 cm^{-1} were determined from the curve fits of the Raman spectra acquired at the onset of the HT, as depicted in Fig. 7. Before 100 °C, it is already possible to determine the peak area at 850 cm^{-1}, value which grows quickly from 150 °C reaching a maximum value at 275 °C, revealing that a higher amount of β-MoO_3 phase is reached around this temperature. As in the He-grown sample, the formation of monoclinic phase is caused by the crystallization of the amorphous matrix of this porous sample. After 275 °C, the amount of β-MoO_3 phase decreases rapidly disappearing at 350 °C as revealed by the evolution of the peak area at 850 cm^{-1} between these temperatures. Fig. 7 also reveals that at 275 °C and 300 °C the main phase in the sample is β-MoO_3 since the values of peak area at 850 cm^{-1} in these two temperatures are higher than the ones corresponding to the signal at 820 cm^{-1} associated to α-MoO_3. On the other hand, the decrease of β-MoO_3 phase between 275 and 350 °C is attributed to the conversion of this phase to α-MoO_3. This transformation that leads to a rise of α-MoO_3 phase in the sample is evidenced by the strong increase of the peak area at 820 cm^{-1} after 275 °C. The small decrease of the peak area at 820 cm^{-1} between RT up to 150 °C does not mean a decrease of the amount of α-MoO_3 since it must remain constant until the β-MoO_3 → α-MoO_3 transition occurs. Between RT and 150 °C, the signal at 850 cm^{-1} is very weak and poorly defined, being only a small shoulder at the side of the signal at 820 cm^{-1}. For this reason, the fit leads to a poor estimation of the peak area for this particular signal causing also variations in the value of the peak area of the signal at 820 cm^{-1}.

A non-treated amount of this H_2-grown sample was subjected to the same thermal history up to 325 °C. Then, a HT between 325 °C and 350 °C with a heating rate of 2 °C min^{-1} was performed and in situ Raman spectra were dynamically acquired each 2 °C to determine the temperature of total conversion of the β-MoO_3 phase to α-MoO_3.

Fig. 8 shows Raman spectra in the range of high-wave number, between 600 and 1100 cm^{-1}, for the H_2-grown porous sample treated between 325 and 331 °C. The spectra sequence reveals that the presence of a small proportion of monoclinic phase is still present in the sample up to 327 °C evidenced by the small shoulders centered at 850 and 776 cm^{-1}. At 329 °C these shoulders are no longer detected, however, the peak centered at 820 cm^{-1} appears slightly asymmetric. This peak became more symmetric at 331 °C, a fact attributed to total conversion to α-MoO_3 of the amount of monoclinic phase present in sample at 325 °C.

3.4. Final state of the treated samples

The final effect of the HT on the structure and oxidation state of the porous samples was the same. Highly crystalline material of orthorhombic structure of MoO_3 and an oxide slightly reduced was the final result in both treated samples.

Fig. 9 shows Raman spectra of the H_2-grown sample acquired at RT recorded before (a) and after (b) HT. After the HT, the Raman peaks are more intense and sharp indicating a major amount of highly crystalline phase. In fact, the full width at high maximum (FWHM) of the signal at 820 cm^{-1} before the HT was of 17.9 cm^{-1} whereas the one after HT was of 9.5 cm^{-1}. A slight shift of some Raman signals in the low-wave number range also was detected in the spectrum acquired at RT after HT, as revealed by Fig. 9. The Raman profile of Fig. 9(b) is more seemed to the one acquired from the MoO_3 crystalline powder used as reference sample (see Fig. 1).

The HT up to 450 °C performed in air on both porous samples caused also a slight reduction of molybdenum trioxide. Fig. 10 shows XPS spectra of the Mo 3d photoelectron peaks from the H_2-grown sample acquired (a) before and (b) after the HT. Fig. 10(a) shows the Mo 3d doublet which was fitted with two curves assigning 233.2 eV to the Mo $3d_{5/2}$ and 236.3 eV to the Mo $3d_{3/2}$ peaks, with a full width at half maximum (FWHM) of 2.5 eV and 2.7 eV, respectively. These binding energies are attributed to Mo^{6+}

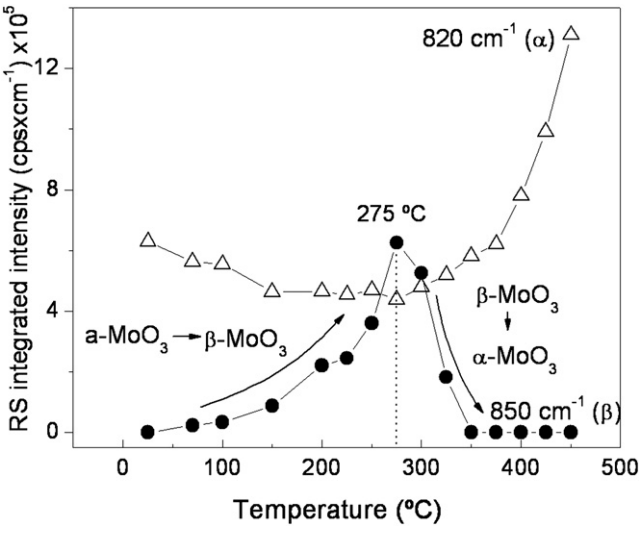

Fig. 7. Evolution of the area below the curve of the peaks located at 850 and 820 cm^{-1} by HT effect.

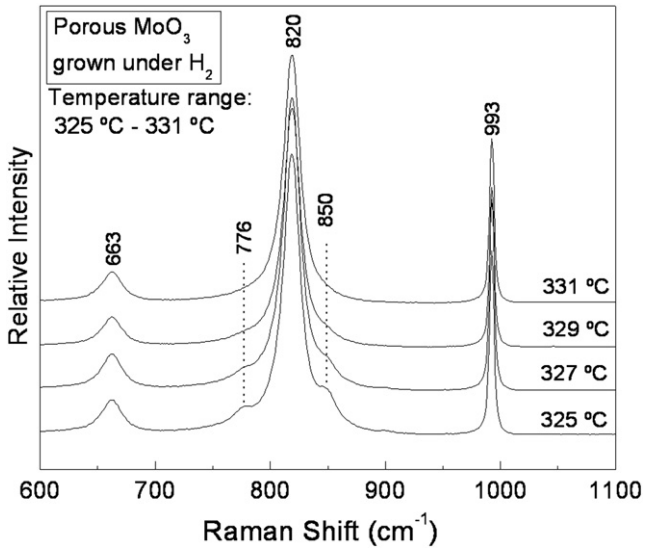

Fig. 8. Raman spectra of the H_2-grown porous sample acquired between 325 and 331 °C

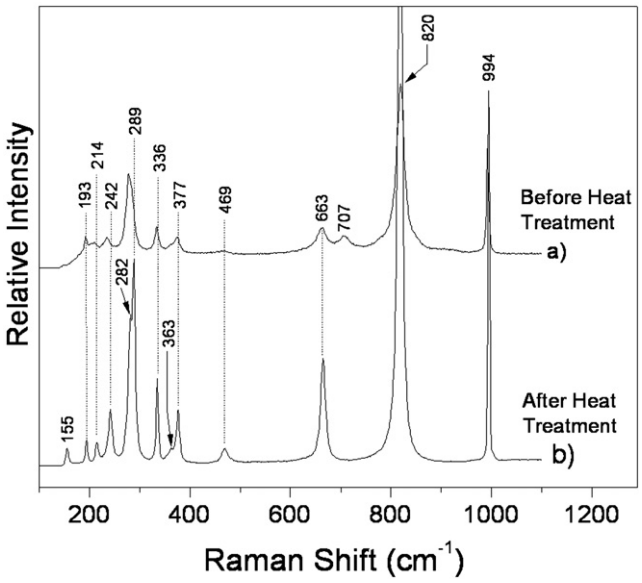

Fig. 9. Raman spectra of the H_2-grown porous sample acquired (a) before and (b) after HT

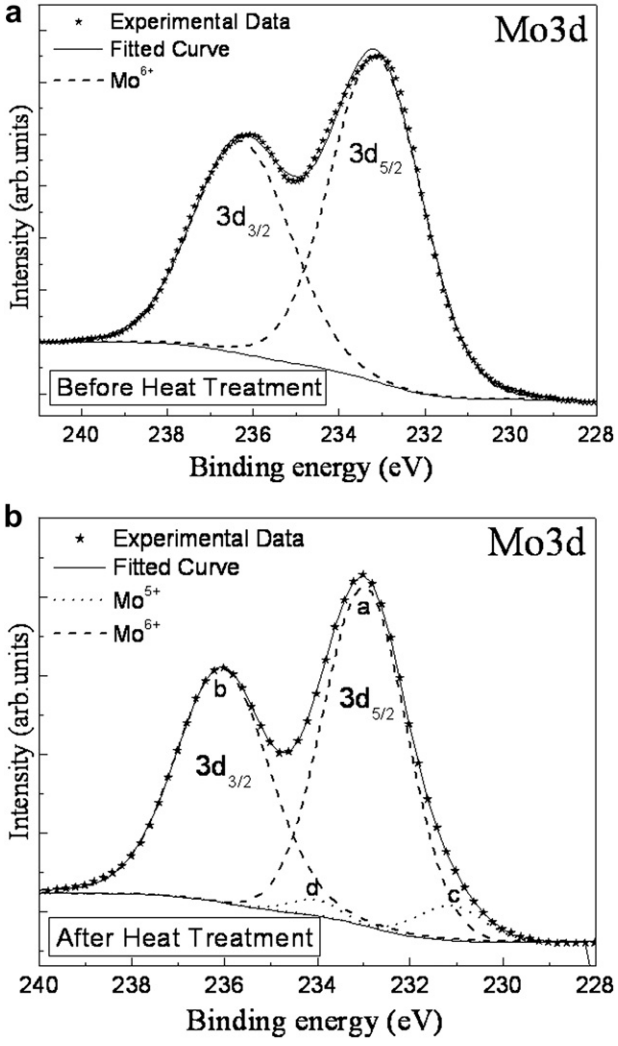

Fig. 10. XPS Mo 3d levels and fit for the H_2-gown porous sample. The spectra were acquired (a) before and (b) after HT.

ions. The spectrum of Fig. 10(b) acquired after the HT shows that the best fit was obtained by means of four overlapping peaks labeled as a, b, c, and d. The binding energies of the higher intensity Mo 3d doublet (peaks a and b) were 233.0 eV (FWHM ~ 2.2 eV) and 236.1 eV (FWHM ~ 2.4 eV) corresponding to Mo^{6+}. The doublet of lower intensity (peaks c and d) was fitted with binding energies of 231.2 eV (FWHM ~ 1.6 eV) and 234.2 eV (FWHM ~ 1.7 eV) for Mo $3d_{5/2}$ and Mo $3d_{3/2}$, respectively. These binding energies are attributed to Mo^{5+} ions revealing, therefore, a slight reduction of MoO_3 after HT.

This interpretation does not depend on the criterion used to fix the energy scale. The key point is the energy difference between the maxima of the two species detected, which in our case amounts to 1.8 eV. This value is slightly closer to the 2.1 eV of separation between the peaks attributed to Mo(VI) and Mo(V) reported by T. Sian and G. Reddy [34] for amorphous films than the 1.3 eV reported by C.V. Ramana et al. [35] for polycrystalline films.

3.5. Results summary

Table 1 shows a summary with the main results from each sample. The reference sample, MoO_3 crystalline powder, does not exhibit structural transformations after 105 min of laser irradiation or the HT up to 450 °C whereas the porous samples underwent important structural changes. These structural changes were mainly associated to the structure transition of the starting amorphous matrix. However, the temperature ranges of the structural transitions were very different, in special, the one associated to the first phase change from amorphous MoO_3 to β-MoO_3, as shown in Table 1, evidencing the different thermal stability of each amorphous matrix.

4. Discussion

The difference in stability under laser irradiation between the He and H_2-grown samples can be attributed to the onset of crystallization of the amorphous matrix. E. Haro-Poniatowski et al. reported that a laser power density of the order of 15 W mm^{-2} was necessary to induce the crystallization of a hydrated amorphous MoO_3 [27], which in our case reduces to only 0.7 W mm^{-2} for the H_2-grown sample. The metastability of this amorphous phase is of interest for the optical recording area, since this material could be used as a high density optical storage medium. Moreover, the crystallinity of this porous material could be finely tuned using the laser-annealing technique. This would be useful for fabricating MoO_3 films with different crystalline quality and use them as cathode in solid-state lithium microbatteries, since the lithium intercalation process depends strongly on the crystallinity of the films [36].

Our value of 250°—275° for the temperature of the amorphous-monoclinic transition of the He-grown samples is in the range reported in the literature: 250 °C in ref. [16], 280 °C in ref. [32]. On the other hand, the H_2-grown samples experiment the same transition at lower temperatures, with an onset at 70 °C. This is consistent with the rapid structural transformations induced by laser irradiation. Porous MoO_3 grown in hydrogen contains a high concentration of OH groups [24]. We guess that the release of hydrogen contained inside the sample and the break of weak bonds between Mo atoms and OH groups would promote the early transformation of the H_2-grown sample. The high conversion rate of the amorphous phase between 200 and 275 °C could be promoted by a dehydration process of the amorphous phase since the as-received H_2-grown sample was slightly hydrated. In a previous research, D.E. Diaz-Droguett et al. found by thermogravimetric analysis that the removal of the lattice H_2O molecules

Table 1
Main results obtained from each sample.

Samples	Structural transformations induced by laser irradiation	Structural transformations induced by heat treatment	Temperature range of the onset of the transition α-MoO_3 → β-MoO_3	Temperature range of the onset of the transition β-MoO_3 → α-MoO_3
MoO_3 powder	No	No	–	–
He-grown porous MoO_3	No	Yes	250 °C–275 °C	300 °C–325 °C
H_2-grown porous MoO_3	Yes	Yes	25 °C–70 °C	275 °C–300 °C

from H_2-grown porous samples at 100 Pa occurs between 220 and 260 °C [24].

At 325 °C the He-grown β-MoO_3 phase starts to convert to α-MoO_3, a process completed at 350 °C. These temperatures are slightly lower to the literature values of 350 °C reported in [16] and 400 °C reported in [14,32,37]. The H_2-grown β-MoO_3 phase transforms to α-MoO_3 in the interval 275 °C to 300 °C.

5. Conclusions

MoO_3 porous material prepared by evaporation of MoO_3 under helium or hydrogen atmosphere at 100 Pa showed significant differences in its structure stability by heating effects. In both type of samples, the thermally induced structural changes were mainly associated to the phase transformations of their starting amorphous matrix. The He-grown sample was stable under the laser irradiation of 105 minutes presenting structure transformations only above 250 °C. In fact, the conversion of its amorphous phase to β-MoO_3 started between 250 °C and 275 °C. On the contrary, the crystallization onset of the amorphous phase to β-MoO_3 for the H_2-grown sample occurred at very low temperatures, between 27 °C and 70 °C (Table 1). The metastability of the H_2-grown sample was initially evidenced by the experiments using only laser irradiation where changes in the Raman spectra were detected at barely 10 min of irradiation.

Under HT, the transition of the formed β-MoO_3 phase to α-MoO_3 occurred in both samples at similar temperatures, between 300 °C and 325 °C for the He-grown sample and between 275 °C and 300 °C for the H_2-grown sample.

Acknowledgments

D.E. Diaz-Droguett acknowledges to the Postdoctoral Fondecyt project No. 3110035 for financial support and to Department of Physics of Pontificia Universidad Católica de Chile (PUC-Chile).

References

[1] K. Ishizaki, S. Komarneni, M. Nanko, Porous Materials: Process Technology and Applications, Kluwer Academic Publishers, Dordrecht, 1998.
[2] B.B. Lakshmi, C.J. Patrissi, C.R. Martin, Chem. Mater. 9 (1997) 2544–2550.
[3] C.N.R. Rao, B. Raveau, Transition Metal Oxides: Structure, Properties, and Synthesis of Ceramic Oxides, second ed. Wiley-VCH, United States of America, 1998, p. 230.
[4] R.K. Grasselli, Catal. Today 49 (1999) 141–153.
[5] M.M. Bettahar, G. Costentin, L. Savary, J.C. Lavalley, Appl. Catal. A 145 (1996) 1–48.
[6] J. Haber, E. Lalik, Catal. Today 33 (1997) 119–137.
[7] A.M. Taurino, A. Forleo, L. Francioso, P. Siciliano, M. Stalder, R. Nesper, Appl. Phys. Lett. 88 (2006) 1–3.
[8] N. Miyata, T. Suzuki, R. Ohyama, Thin Solid Films 282 (1996) 218–222.
[9] E. Comini, G. Faglia, G. Sberveglieri, C. Cantalini, M. Passacantando, S. Santucci, Y. Li, W. Wlodarski, W. Qu, Sens. Actuators B 68 (2000) 168–174.
[10] C. Fukushima, M. Nagano, T. Sumita, H. Kubota, M. Nagata, Y. Honda, T. Oku, J. Imahori, Physica B 239 (1997) 56–58.
[11] C. Imawan, H. Steffes, F. Solzbacher, E. Obermeier, Sens. Actuators B 78 (2001) 119–125.
[12] O. Merdrignac-Conanec, P.T. Moseley, Electrochem. Commun. 1 (1999) 51–54.
[13] S.S. Sunu, E. Prabhu, V. Jayaraman, K.I. Gnanasekar, T.K. Seshagiri, T. Gnanasekaran, Sens. Actuators B: Chem. 101 (2004) 161–174.
[14] B. Yebka, C. Julien, G.A. Nazri, Mater. Sci. Eng. B 38 (1996) 65–71.
[15] H.M. Kim, T. Fukumoto, S. Hayashi, K. Yamamoto, J. Phys. Soc. Jpn. 63 (1994) 2194–2201.
[16] I. Juárez Ramírez, A. Martínez-de la Cruz, Mater. Lett. 57 (2003) 1034–1039.
[17] B. Baker, T.P. Feist, E.M. McCarron III, J. Solid State Chem. 119 (1995) 199–202.
[18] V.V. Atuchin, T.A. Gavrilova, V.G. Kostrovsky, L.D. Pokrovsky, I.B. Troitskaia, Inorganic Mater. 44 (2008) 622–627.
[19] C.V. Ramana, I.B. Troitskaia, V.V. Atuchin, M. Ramos, D. Ferrer, J. Vac. Sci. Technol. A 28 (2010) 726–729.
[20] A. Michalak, K. Hermann, M. Witko, Surf. Sci. 366 (1996) 323–336.
[21] R. Tokarrz-Sobieraj, K. Hermann, M. Witko, A. Blume, G. Messtl, Surf. Sci. 489 (2001) 107–125.
[22] J.B. Parise, E.M. McCarron, R. Von Dreele, Solid State Chem. 93 (1991) 193–201.
[23] D.E. Díaz-Droguett, V.M. Fuenzalida, M.S. Díaz-Espinoza, G. Solórzano, J. Mater. Sci. 43 (2008) 591–596.
[24] D.E. Díaz-Droguett, V.M. Fuenzalida, Mater. Chem. Phys. 126 (2011) 82–90.
[25] R. Murugan, A. Ghule, C. Bhongale, H. Chang, J. Mater. Chem. 10 (2000) 2157–2162.
[26] M.A. Camacho-López, E. Haro-Poniatowski, L. Lartundo-Rojas, J. Livage, C.M. Julien, Mater. Sci. Eng. B 135 (2006) 88–94.
[27] E. Haro-Poniatowski, C. Julien, B. Pecquenard, J. Livage, M.A. Camacho-López, J. Mater. Res. 13 (1998) 1033–1037.
[28] S. Wang, Y. Zhang, W. Wang, G. Li, X. Ma, X. Li, Z. Zhang, Y. Qian, J. Cryst. Growth 290 (2006) 96–102.
[29] M. Dieterle, G. Weinberg, G. Mestl, Phys. Chem. Chem. Phys. 4 (2002) 812–821.
[30] V.V. Atuchin, T.A. Gavrilova, T.I. Grigorieva, N.V. Kuratieva, K.A. Okotrub, N.V. Pervukhina, N.V. Surovtsev, J Cryst. Growth 318 (2011) 987–990.
[31] M.A. Camacho-López, L. Escobar-Alarcón, M. Picquart, R. Arroyo, G. Córdoba, E. Haro-Poniatowski, Optical Mater. 33 (2011) 480–484.
[32] E. McCarron III, J. Chem. Soc., Chem. Commun. 4 (1986) 336–338.
[33] G. Mestl, P. Ruiz, B. Delmon, H. Knözinger, J. Phys. Chem. 98 (1994) 11269–11275.
[34] T.S. Sian, G.B. Reddy, Solar Energy Mater. Solar Cells 82 (2004) 375–386.
[35] C.V. Ramana, V.V. Atuchin, V.G. Kesler, V.A. Kochubey, L.D. Pokrovsky, V. Shutthanandan, U. Becker, R.C. Ewing, Appl. Surf. Sci. 253 (2007) 5368–5374.
[36] C. Julien, A. Khelfa, J.P. Guesdon, A. Gorenstein, Appl. Phys. A 59 (1994) 173–178.
[37] J.R. Gunter, J. Solid State Chem. 5 (1972) 354–359.